J Appl Physiol 106: 813–822, 2009.
First published November 20, 2008; doi:10.1152/japplphysiol.01133.2007.

The difference in ventilation heterogeneity between asthmatic and healthy subjects quantified using hyperpolarized ^{3}He MRI

Yang-Sheng Tzeng,[1,2] Kenneth Lutchen,[2] and Mitchell Albert[1,3]

[1]*Department of Radiology, Brigham & Women's Hospital, Boston;* [2]*Department of Biomedical Engineering, Boston University, Boston; and* [3]*Department of Radiology, University of Massachusetts Medical School, Worcester, Massachusetts*

Submitted 23 October 2007; accepted in final form 17 November 2008

Tzeng YS, Lutchen K, Albert M. The difference in ventilation heterogeneity between asthmatic and healthy subjects quantified using hyperpolarized ^{3}He MRI. *J Appl Physiol* 106: 813–822, 2009. First published November 20, 2008; doi:10.1152/japplphysiol.01133.2007.—In this pilot study, algorithms for quantitatively evaluating the distribution and heterogeneity of human ventilation imaged with hyperpolarized (HP) ^{3}He MRI were developed for the goal of examining structure-function relationships within the asthmatic lung. Ten asthmatic and six healthy human subjects were imaged with HP ^{3}He MRI before bronchial challenge (pre-MCh), after bronchial challenge (post-MCh), and after a series of deep inspirations (post-DI) following challenge. The acquired images were rigidly coregistered. Local voxel fractional ventilation was computed by setting the sum of the pixel intensity within the lung region in each image to 1 liter of inhaled ^{3}He mixture. Local ventilation heterogeneity was quantified by computing regional signal coefficient of variation. Voxel fractional ventilation histograms and overall heterogeneity scores were then calculated. Asthmatic subjects had a higher ventilation heterogeneity to begin with ($P = 0.025$). A methacholine challenge elevated ventilation heterogeneity for all subjects (difference: $P = 0.08$). After a DI postchallenge, this heterogeneity reversed substantially toward the baseline state for healthy subjects but only minimally in asthmatic subjects. This difference was significant in absolute quantity (difference: $P = 0.007$) as well as relative to the initial increase (difference: $P = 0.03$). These findings suggest that constriction heterogeneity is not a characteristic unique to asthmatic airway trees but rather a behavior intrinsic to all airway trees when provoked. Once ventilation heterogeneity is established, it is the lack of reversal following DIs that distinguishes asthmatics from non-asthmatics.

RECENT STUDIES HAVE EMPHASIZED two distinguishing features of asthmatic lungs. First, when provoked, these airways constrict heterogeneously (14). Second, when bronchoconstricted, asthmatics tend to be less responsive to deep inspirations (DI) than healthy subjects (5, 13). In fact, it was noted by Skloot (40) that one could substantially amplify airway reactivity in otherwise healthy lungs simply by prohibiting DIs for extended periods of time. These phenomena motivate the need for a more comprehensive understanding of heterogeneous airway constriction in the context of asthmatic versus healthy airways and how they respond to DIs. However, the tools used to study ventilation heterogeneity in humans, the measurement of lung mechanics (26–27) and multiple-breath inert gas washout (23–25, 41, 43), provide only global and implicit assessment of the functional impact of structural changes.

Since airways constitute the paths by which ventilation reaches the alveoli, heterogeneous narrowing of the airways should lead to correspondingly nonuniform ventilation. This study was motivated by the overriding hypothesis that airway provocation will result in ventilation heterogeneity in both healthy and asthmatic subjects, but only asthmatics will display a lack of ventilation recovery in response to a deep inspiration. This hypothesis, if proven, will reinforce the notion that whereas provocation of both healthy and asthmatic airways naturally leads to heterogeneous constriction, only asthmatic airways converge to a stiffer condition such that DIs are less effective in resolving the heterogeneity. Image-based methods have the potential to provide quantitative information on the spatial characteristics and heterogeneity of ventilation. To date, however, heterogeneity mostly has been assessed by computing global values of coefficient of variation (CoV) or variance, with several examples in ventilation imaging alone (15, 29, 31, 34–35, 46, 48). These approaches ignore the apparent "local" characteristic of the inhomogeneity that is clearly visible. Furthermore, no imaging effort has tried to capture the effects of DIs on existing ventilation heterogeneity and compare how this behavior differs between healthy and asthmatic subjects.

Imaging techniques for mapping ventilation such as computed tomography (CT) (28) and positron emission tomography (PET) (30) have the drawback of ionizing radiation exposure. Hyperpolarized (HP) ^{3}He MRI (8, 22, 38), however, utilizes no ionizing radiation, and published images to date clearly convey the existence of patchy ventilation defects distributed throughout the lung in bronchoconstricted subjects. Assessments of ventilation have mostly been by subjective scoring or by identifying and/or counting the number of defects (6–8, 17), and comments on their homogeneity/heterogeneity have remained qualitative in nature (2, 4, 22, 37, 39). Combining the wash-in approach with HP ^{3}He MRI to quantitatively map ventilation (10), while rigorous, cannot be readily extended to human studies because of the quantity and cost of the ^{3}He gas necessary, as well as higher safety demands.

In this pilot study we propose approaches to quantifying ventilation and its heterogeneity using HP ^{3}He MRI in a manner applicable to human subjects. Interrogating imaging data with impartial algorithms reduces the uncertainties associated with human judgment. The numerical methods developed in this study were applied to HP ^{3}He ventilation MR images acquired from healthy and asthmatic subjects, to quantify ventilation and characterize the associated heterogeneity in these two subject populations at baseline, following bronchoprovocation, and after DIs. The effect of DIs was further examined in both absolute and relative terms.

Address for reprint requests and other correspondence: M. Albert, 55 Lake Ave, North, Worcester, MA 01655 (e-mail: mitchell.albert@umassmed.edu).

The costs of publication of this article were defrayed in part by the payment of page charges. The article must therefore be hereby marked "*advertisement*" in accordance with 18 U.S.C. Section 1734 solely to indicate this fact.

MATERIALS AND METHODS

Subject enrollment. The Health Insurance Portability and Accountability Act-compliant research protocol in this study was approved by the local Institutional Review Board. Written informed consent was obtained from all recruited subjects. Data were obtained from 10 asthmatic (5 male, 5 female) and six healthy (3 male, 3 female) subjects.

Asthmatics sought for this study were those with mild to moderate asthma, defined as diagnosed asthmatics having a forced expiratory volume in 1 s (FEV_1) $\geq$ 60% predicted without inhaled or oral steroids, asthma symptoms fewer than seven times a week requiring β_2-agonist use, and well-controlled on a low-dose regimen of inhaled corticosteroids (32). Asthmatic subjects were diagnosed based on the dose of methacholine (MCh) at which they achieve a 20% drop in FEV_1 (PC_{20}) (1). Only data from subjects whose PC_{20} value on the day of the MRI experiment continue to satisfy the American Thoracic Society definition of asthmatics are included in this analysis.

Healthy subjects were nonsmokers with no history of respiratory disease. All had a PC_{20} value >25 mg/ml during their asthma screening.

Hardware. MR imaging was carried out on a General Electric Signa LX 1.5T MRI scanner, with a heterodyne system appended to enable imaging at the ^{3}He frequency, and using a flexible quadrature wrap-around lung coil (Clinical MR Solutions, Brookfield, WI) tuned to the ^{3}He frequency. ^{3}He was hyperpolarized to 10–20% via collision spin exchange with optically pumped rubidium (19) using a polarizer built in-house.

Protocol. Scans to acquire static ventilation images of the lung were initiated immediately upon subjects holding their breath after inhaling ~1 liter of ~33% HP ^{3}He-67% N_2 mixture from functional residual capacity. The 1-liter gas mixture volume was ensured with the use of 1-liter Tedlar bags. The scans employed a Fast Gradient Echo pulse sequence acquiring coronal multislice images with a 46-cm field of view (FOV), 0.75 phase FOV, 128 × 256 matrix (zero-padded to 256 × 256), 13-mm slice thickness, 0-mm gap between slices, 31.25-kHz bandwidth, 14–18° flip angle, TE/TR 1.228 ms/50–75 ms, and interleaved data acquisition. Scans ranged from 5 to 10 s, depending on the anterior-posterior depth of the lungs, which may require 9–14 slices to encompass.

Before each scan, a manual prescan at the ^{3}He frequency was carried out to examine the functionality of the heterodyne system and to ensure that no HP ^{3}He signal survived from the previous scan. In the event residual HP ^{3}He signal was detected, manual prescan was continued until the signal was consumed to a negligible degree.

Before the experiments, subjects were asked to withhold caffeine consumption from the beginning of the day. Asthmatic subjects must not have used any fast-acting β_2-agonist inhalers for at least 8 h and any long-acting β_2-agonist inhalers for at least 48 h.

After baseline spirometry (Microlab 3000 Series or Microloop 3535S; Micro Medical) and HP ^{3}He MR imaging, subjects underwent a MCh challenge with the five-breath dosimeter protocol (1) in a seated upright position (DSM2030 Dosimeter and DeVilbiss 646 Nebulizer; S&M Instrument). Briefly, each subject inhaled five deep breaths of a MCh solution at a given concentration and waited for 3 min, at which time the pulmonary status of the subject's lungs was assessed before moving on to the next MCh concentration. The nominal MCh concentrations administered were 0.0, 0.078, 0.156, 0.3125, 0.625, 1.25, 2.5, 5.0, 10.0, and 25.0 mg/ml. Every other MCh concentration in the challenge could be skipped until 10.0 mg/ml for healthy subjects or until the concentration one order of magnitude below the known PC_{20} dose for asthmatic subjects. For asthmatic subjects, the MCh challenge ended upon causing a >20% drop in FEV_1. Because withholding DIs could elicit amplified airway constriction even from nonasthmatics (3, 40), healthy subjects were asked to refrain from taking DIs (including spirometry) after each dose. For healthy subjects, the end point of the MCh challenge was either when the 25 mg/ml dose was reached or upon verbal expression by the subjects that they were experiencing significant chest tightness. Subjects then went through the second HP ^{3}He MR imaging.

Returning the table of the MRI scanner back to its home position, subjects were instructed to sit up and take 3–5 DIs, with a 3- to 5-s breathhold at the end of the last DI. The seated position is for consistency with spirometry and MCh challenge. Afterward, subjects were reinserted into the MRI, upon which the third HP ^{3}He MR imaging procedure was conducted. The anterior-posterior coordinates for the post-MCh and post-DI MRI scans were the same as those used for the baseline/pre-MCh scan.

Subjects must have returned to at least 90% of their baseline FEV_1 before being released from the experiment session. In the event this recovery did not occur spontaneously after the post-DI data acquisition, albuterol was used to aid this process.

Quantification of ventilation and heterogeneity. From each session, one set of HP ^{3}He MR images was acquired from each of the experiment's three stages: pre-MCh, post-MCh, and post-DI. For each coronal slice, the post-MCh image and post-DI image were coregistered to the corresponding pre-MCh image by identifying the maximum of the normalized two-dimensional (2-D) cross-correlation function within a ±32-pixel translation in the craniocaudal direction and a ±16-pixel translation in the left-right direction. The results of the automatic, rigid coregistration were visually inspected, and final manual adjustments may be carried out.

For each slice, the lung regions of interest (ROI) were manually traced from the pre-MCh image. The same regions were considered as the lungs in the post-MCh and post-DI data sets. Manual definition of the lung ROI, as opposed to a more automated thresholding approach, is necessary to avoid leaving out from the analysis regions of the lung that are poorly ventilated or unventilated even before bronchial challenge, particularly in asthmatics. The combination of coregistration and application of pre-MCh lung ROIs to post-MCh and post-DI data sets enables the comparison of the same lung regions across the different stages of the experiment. The pixel intensities of the pixels outside the lung ROI were set to zero. The mean noise level of an image was subtracted from all the pixel intensities (16, 20) within the lung ROI of that slice. Negative resulting pixel intensities were set to zero. C, a signal intensity-to-volume conversion factor, was computed by equating the resulting pixel intensity sum for each stage of the experiment with 1 liter of inhaled ^{3}He-N_2 mixture.

$$C = \frac{1}{\sum S_{i,j,k}} \quad (1)$$

where S is the resulting pixel intensity, i and j are the pixel indexes, and k is the coronal slice index. The volume fraction of each voxel occupied by the ^{3}He mixture then followed as

$$R_{i,j,k} = \frac{C \cdot S_{i,j,k}}{V_{voxel}} \quad (2)$$

where V_{voxel} is the volume of each voxel. In addition, histograms of voxel volume fraction occupied by ^{3}He for the entire lung were constructed, and each histogram element was normalized such that their sum came to 1.0. Hereafter, the voxel volume fraction occupied by ^{3}He will be referred to as the voxel fractional ventilation ($R_{i,j,k}$).

Defining the global length scale for the lungs as the average of the left and right lungs' maximum width, the local length scale L was then defined to be 10% of the global length scale. For each pixel within the lung ROI, a heterogeneity index $H_{i,j,k}$ was calculated by computing the CoV of the voxel fractional ventilation in its neighborhood. The neighborhood of a pixel in the lung ROI is defined as the pixels within a square (inclusive) of sides L centered around the pixel, in the same slice as the pixel of interest. Pixels outside the lung ROI are excluded from the neighborhood. For pixels whose neighborhoods are dominated by ventilation defects, the computed CoV would be more

indicative of noise characteristics than actual ventilation heterogeneity. Thus pixels whose neighborhood had an overall signal-to noise ratio (SNR) less than two were excluded from the computation of heterogeneity indexes, as well as subsequent computation of heterogeneity scores. A heterogeneity score $\hat{H}$ for each image set was obtained by averaging the $H_{i,j,k}$ values for the entire image set. The changes in $\hat{H}$ after the MCh challenge and after the DIs were computed.

$$\Delta H_{MCh} = \hat{H}_{post\text{-}MCh} - \hat{H}_{pre\text{-}MCh} \quad (3a)$$

$$\Delta H_{DI} = \hat{H}_{post\text{-}DI} - \hat{H}_{post\text{-}MCh} \quad (3b)$$

Finally, the recovery index,

$$Q = -\frac{\hat{H}_{post\text{-}DI} - \hat{H}_{post\text{-}MCh}}{\hat{H}_{post\text{-}MCh} - \hat{H}_{pre\text{-}MCh}} \times 100\% \quad (4)$$

was computed for each subject to examine how much of the elevated heterogeneity resulting from bronchoprovocation subsides with the DIs.

During the coregistration of images, plotting of voxel fractional ventilation histograms, and computation of heterogeneity scores, the trachea and discernible major airways were manually excluded. All algorithms were implemented in MatLab version 6.0.0.88 release 12 (The Mathworks, Natick, MA).

Statistical analysis. The changes in the heterogeneity scores from pre-MCh to post-MCh and from post-MCh to post-DI and the recovery index for both asthmatic and healthy subject populations were evaluated using a two-tailed Student's *t*-test. A two-sample Student's *t*-test was used to examine the differences in MCh-induced increases in heterogeneity score, DI-facilitated changes in heterogeneity score, and recovery indexes between the two subject populations. Welch's corrections were applied to the *t*-tests to not assume equal variances among the subject groups, and $P \leq 0.05$ was considered statistically significant.

Interuser variability. The data processing was repeated by two individuals other than the lead author to examine the interuser variability of the data processing approach. Data from three randomly selected healthy subjects and three randomly selected asthmatic subjects were used for this exercise. Results from the repeated data processing, including the manually defined ROI for each lung slice, the voxel fractional ventilation histograms, and overall heterogeneity scores for each of the three stages of the experiments, were compared against the original results from the lead author. For ROI definition, the sum of the pixel selection false positives and false negatives of the two repeat efforts were divided by the sum of pixels in the original effort. Differences in heterogeneity scores between the repeated and the original computed scores were also divided by the original computed scores. These enabled the differences to be viewed as a percentage of the original results. Repeat voxel fractional ventilation histograms were visually compared against the original histograms to examine whether the originally observed trends were preserved.

RESULTS

Relevant subject information is tabulated in Table 1. The reported PC_{20} values are those recorded from the MCh challenge on the day of the experiment. None of the healthy subjects reported discomforts to end the MCh challenge before the 25 mg/ml dose. The SNR information provided for each subject spans all the images from all three stages of the experiment. SNR values were computed with the signal evaluated from regions that encompass both ventilated and unventilated regions of the lung, to prevent bias due to ventilation pockets or defects.

Figures 1 and 2 show the original images (negatives instead of positives are used to aid the reader in visualizing imaged features), the corresponding voxel fractional ventilation maps, and the resulting heterogeneity maps. Figure 1 shows these depictions for a healthy subject, and Fig. 2 shows the corresponding information for an asthmatic subject. The quantitative ranges indicated by the color bars apply to both the ventilation and heterogeneity maps. At baseline, the HP ^{3}He MR ventilation images indicate that most lung voxels are 10–40% occupied by HP ^{3}He (Fig. 1*b1*), and the cool colors in the corresponding heterogeneity map reflects the high homogeneity. However, after the MCh challenge, voxel fractional ventilation clearly became more heterogeneous, accentuated by pockets of very enhanced voxel fractional ventilation (warmer colors) and areas of voxel fractional ventilation deprivation (colder colors) (Fig. 1*b2*); the number of voxels 10–40% occupied by ^{3}He was reduced, accompanied by minimal increases in the number of voxels occupied by 50–80% ^{3}He and

Table 1. *Pertinent information on subjects who participated in this study*

Subject	Sex, M/F	Age, yr	Height, cm	PC_{20}, mg/ml	Baseline FEV_1, %predicted	Asthma Medications	SNR Range of Images
				Healthy subjects			
HEAL1	M	22	180	N/A	95.2	N/A	17–46
HEAL2	F	23	165	N/A	115	N/A	19–50
HEAL3	F	25	150	N/A	103	N/A	21–42
HEAL4	M	47	155	N/A	117	N/A	7–14
HEAL5	F	24	155	N/A	94.9	N/A	23–57
HEAL6	M	23	183	N/A	99.3	N/A	15–46
				Asthmatics subjects			
RA1	F	34	160	<0.078	90.2	Ventolin PRN as needed	15–44
RA2	F	22	168	2.041	104	Advair, Albuterol 2-3 times/day	23–50
RA3	M	45	180	0.096	89.0	Primatene mist as needed	15–39
RA4	M	23	173	1.915	78.1	Advair 250/50 5 puffs/day	18–53
RA5	F	29	168	0.798	83.9	Advair 100/50 2 puffs/day, Albuterol as needed	14–40
RA6	M	27	180	2.183	79.0	Albuterol as needed, Flovent 1-2 times/yr	13–37
RA7	M	21	178	0.269	84.2	Albuterol as needed	6–31
RA8	F	45	165	0.780	69.9	Albuterol as needed	9–42
RA9	M	22	188	0.174	82.6	Albuterol as needed	6–25
RA10	F	22	163	1.112	96.6	Albuterol as needed	9–49

M/F, male or female; FEV_1, forced expiratory volume in 1 s; PC_{20}, dose of methacholine resuting in a 20% drop in FEV_1; SNR, signal-to-noise ratio; N/A, not applicable.

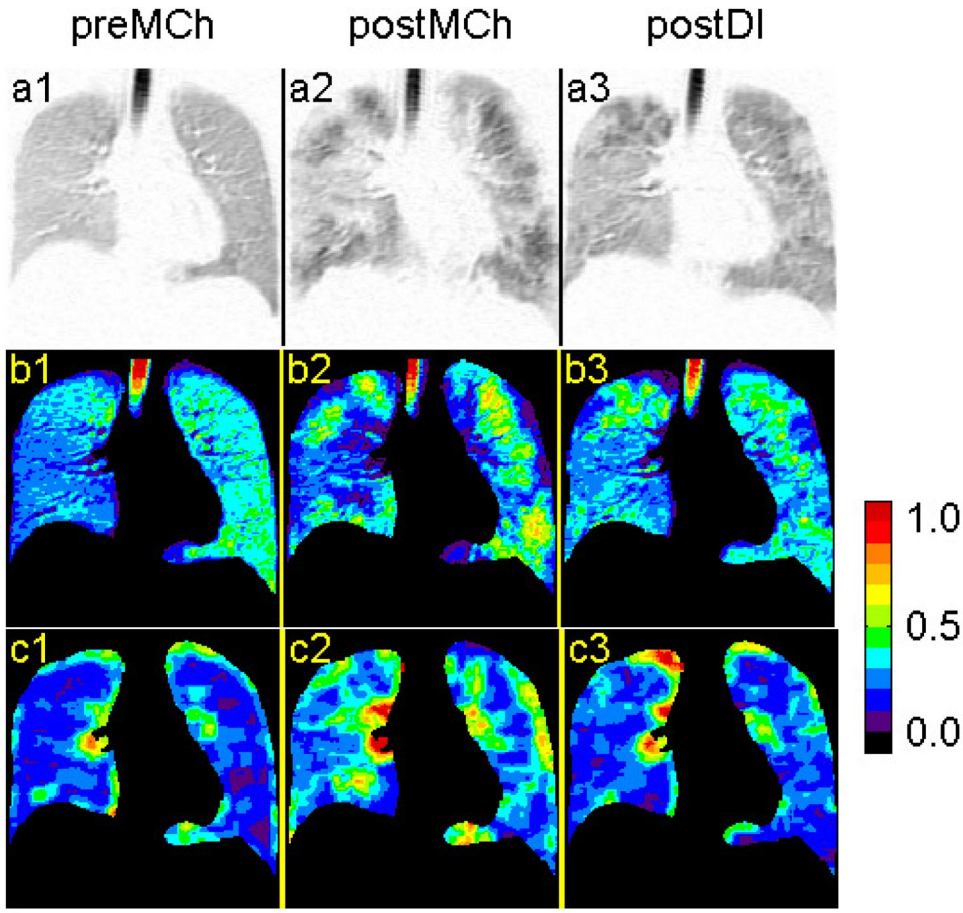

Fig. 1. Images from healthy subject *HEAL3*, coronal slice 5 of 10. Original images (*a1*–*a3*), voxel fractional ventilation ($R_{i,j,k}$) maps (*b1*–*b3*), and heterogeneity ($H_{i,j,k}$) maps (*c1*–*c3*) are shown before methacholine challenge (pre-MCh), after MCh challenge (post-MCh), and after deep inspirations (post-DI). Quantitative ranges indicated by the color bar apply to both the ventilation and heterogeneity maps.

a larger increase in the number of voxels that contained <10% ^{3}He by volume. The heterogeneity images also show widespread local variability in voxel fractional ventilation (Fig. 1*c2*). After taking DIs, these healthy subjects were able to rehomogenize much of the voxel fractional ventilation (Fig. 1, *a3*, *b3*, and *c3*). Indeed, post-DI, the images are visually very similar to those at baseline.

Some asthmatic subjects had preexisting elevation of ventilation heterogeneity, as shown in Fig. 2, *a1* and *b1*. Similar to healthy subjects, voxel fractional ventilation became more heterogeneous (Fig. 2, *a2*, *b2*, and *c2*) after MCh challenge. However, unlike healthy subjects, DIs appeared to have little impact on ventilation heterogeneity in asthmatic lungs (Fig. 2, *a3*, *b3*, and *c3*).

Figure 3 plots the voxel fractional ventilation histograms for four subjects at each of the three stages of the experiment. In all subjects, the histograms become more spread out following the MCh challenge. Substantial percentages of voxels with near-zero ventilation now exist, in contrast to negligible quantities at baseline. Consistent with the voxel fractional ventilation and heterogeneity maps, DIs moved these distributions back toward pre-MCh conditions in healthy subjects but not in the asthmatics.

For any one condition, the heterogeneity score over the entire set of images was calculated, and results for individual subjects at each of the three experiment stages are tabulated in Table 2. The overall results across the subjects are plotted in Fig. 4, showing a clear difference between the healthy and asthmatic subject groups at baseline conditions ($P = 0.025$). Figure 5 shows the changes in this index from baseline produced by MCh challenge (a positive change indicates an increase in heterogeneity) and then the subsequent changes from post-MCh to post-DI. For the ventilation heterogeneities of both healthy and asthmatic subjects, the increases due to MCh challenge and reductions following DIs were statistically significant. However, although no difference was found between their MCh-induced heterogeneity increases ($P = 0.08$), these two subject groups clearly differed in the degree to which DIs reduced the established heterogeneity ($P = 0.007$). The recovery index Q (Fig. 6) was also significantly different ($P = 0.03$) between these two subject populations.

The root mean square adjustments after automated rigid coregistration for the subjects were 0.66 pixels in the left-right direction and 3.55 pixels in the craniocaudal direction. For the repeated data processing of the six randomly selected subjects, the mean difference in the definition of individual lung slice ROIs was 7.9%, with a maximum of 17%. The mean difference in the image set heterogeneity scores was 4.4%, with a maximum of 12.2%. Visual comparisons of the histograms showed that the difference in voxel fractional ventilation changes between asthmatic and healthy subjects was preserved regardless of the user.

DISCUSSION

In this pilot study, HP ^{3}He MRI was used to present the first imaging evidence that DIs are effective in reversing broncho-

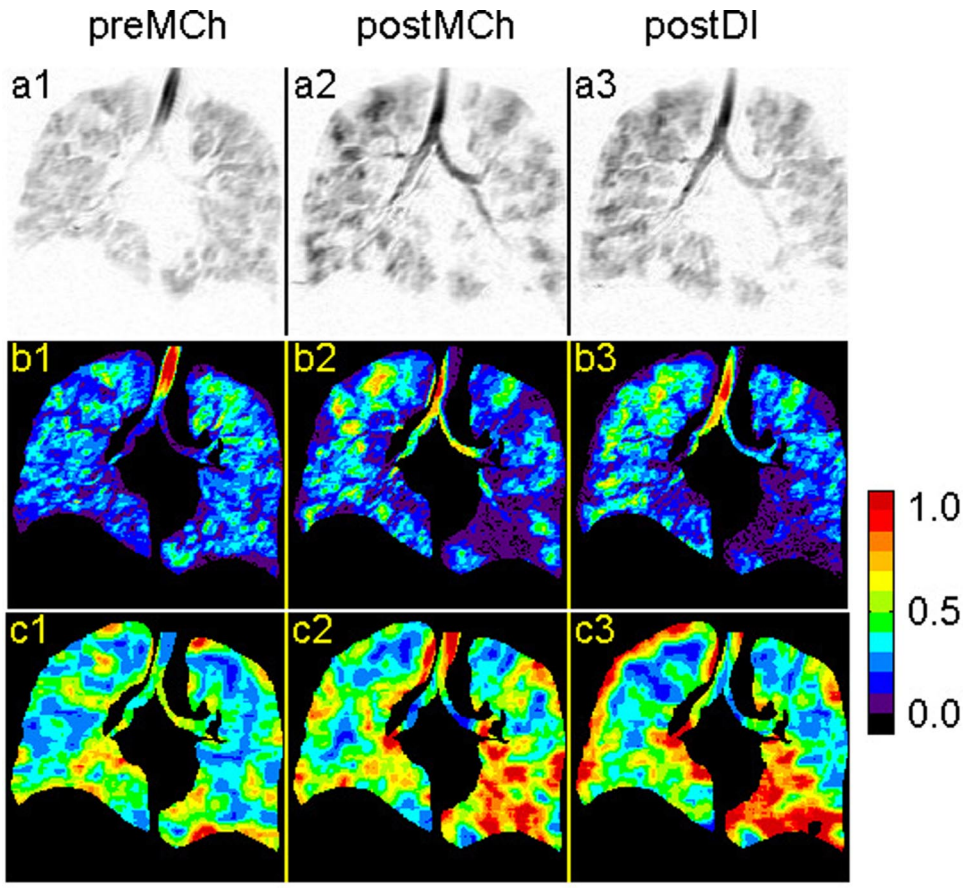

Fig. 2. Images from asthmatic subject *RA1*, coronal slice 6 of 11. (*a1–a3*), voxel fractional ventilation maps (*b1–b3*), and heterogeneity maps (*c1–c3*) are shown pre-MCh, post-MCh, and post-DI. Quantitative ranges indicated by the color bar apply to both the ventilation and heterogeneity maps.

constriction in healthy subjects but are relatively ineffective in asthmatics. Similar degrees of ventilation heterogeneity elevation in asthmatic and healthy subjects as shown in Fig. 5 suggest that heterogeneity is not a characteristic unique to asthma, but rather a behavior intrinsic to all airway trees when provoked. In this respect, it is the lack of reversal (Fig. 5) or recovery (Fig. 6) in ventilation heterogeneity following DIs that distinguishes asthmatics from nonasthmatics. HP ^{3}He MRI therefore demonstrated a defect unique to asthmatics in their ability to create a DI-induced dilation of airways that serves to improve ventilation on subsequent breaths.

Ventilation mapping with HP ^{3}He MRI. Quantification of HP ^{3}He MR images from asthmatics in the past had mostly been achieved by simply searching/counting human/operator-perceived ventilation defects in one image compared with another (2, 6–8, 39). The implication of such approaches is that regional lung ventilation is binary: a lung region is either fully ventilated or devoid of ventilation. This is unsatisfying for our eventual goal of developing a quantitative relation between lung and airway structure and ventilation function. Our proposed method explicitly estimates the fractional volume in each voxel occupied by fresh gas during inhalation. Hence, voxels could be anything from completely empty to completely full of the inhaled gas. The ventilation computed using this method is not the fractional volume of alveoli within the corresponding voxel replaced by fresh gas. That parameter is determined by combining the multiple-breath wash-in technique with HP ^{3}He MRI and has been demonstrated with rodents (10).

Equating the sum of the MR signal to 1 liter of ^{3}He gas stems from the reasoning that the MRI signal sum should correspond to the ^{3}He mixture volume sum of 1 liter. Because individual pixel intensities are normalized by the pixel intensity sum, the accuracy of the 33–67% ^{3}He-N_2 ratio is not critical as long as the images display adequate SNR. Furthermore, it is assumed that oxygen-induced depolarization does not affect the outcome of this analysis significantly. Subjecting HP ^{3}He to 117 and 178 mbar, the lowest and highest levels of local partial pressure of oxygen (P_{O_2}) measured in human lungs (9), for a time span of 10 s, the longest scan time in our experiments, would correspond to a maximum error of ^{3}He volume ratio between two points due to oxygen-induced depolarization. With the use of ^{3}He polarization decay rates set forth by Saam et al. (36), this upper bound was computed to be 30.5% (42).

Although more accurate estimation of initial local ^{3}He polarization is certainly possible (9), such rigor either requires tripling our HP ^{3}He production capacity or limiting data acquisition to just one experiment stage. Although newer methods may acquire both ventilation images and P_{O_2} information within a single scan (11, 12), they cannot cover the entire lung thickness within a single breathhold, a significant drawback since the heterogeneity inherent to asthma implies no region of the lung is representative of others. Because the scientific focus of this study was on the pathophysiology of asthma, we chose to waive acquiring the images that would provide us with the P_{O_2} information. We also should point out that for the length of time needed to perform these scans, the

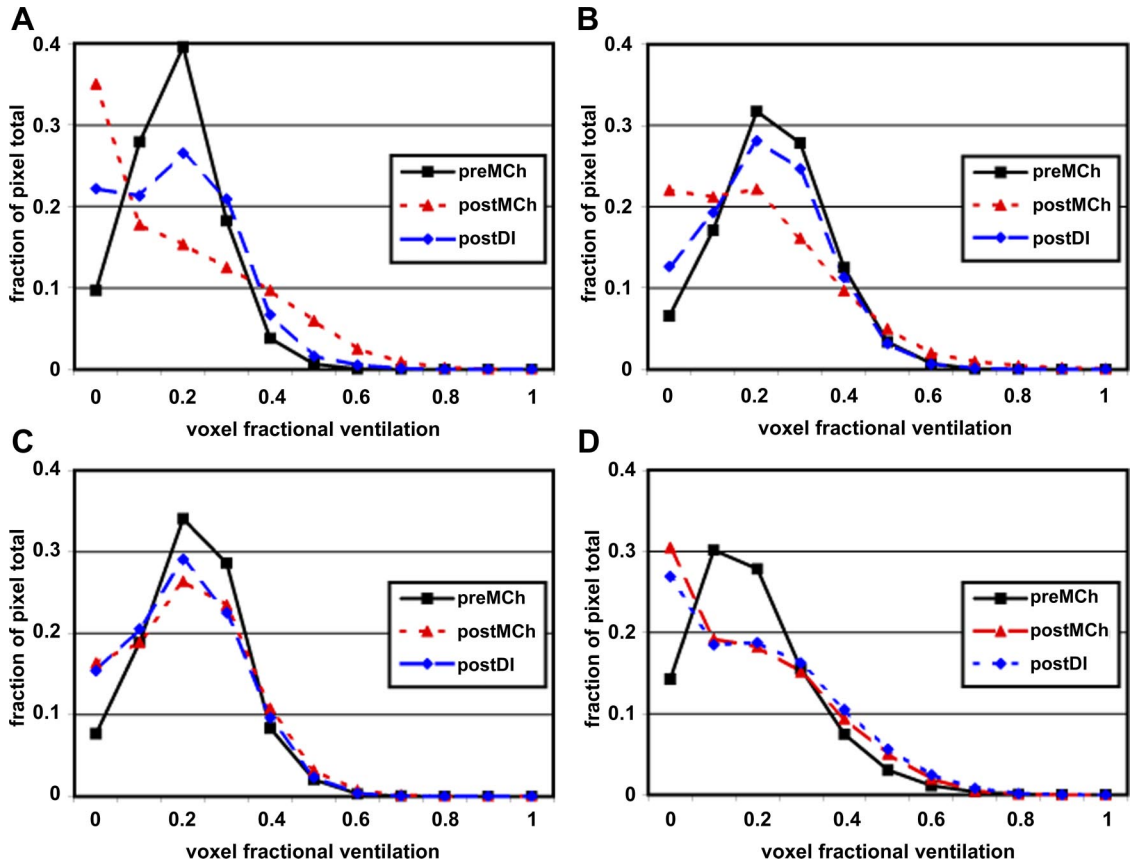

Fig. 3. Voxel fractional ventilation histograms for 4 representative subjects (*A*, HEAL1; *B*, HEAL3; *C*, RA4; *D*, RA8) at each of the 3 experiment stages. It can be clearly seen that DIs were effective in reversing the ventilation of healthy subjects toward their baseline distributions, whereas those of the asthmatic subjects stayed at their bronchially challenged state.

effect of the MCh challenge may wear off in healthy subjects before the data of interest are acquired. On the other hand, the persistence of the bronchoconstriction in asthmatics may lead to discomfort or danger.

Despite the weaknesses of our simplistic ventilation quantification approach, we believe our results demonstrate the effectiveness of this technique in mapping voxel fractional ventilation. Among the supporting evidence is the voxel fractional ventilation distribution across certain sections of the trachea. ^{3}He in the trachea should be least affected by oxygen-induced depolarization. With human tracheal diameter being around 18 mm (21) and avoiding partial volume effects, the contiguous nature of the tracheal space could occupy entire voxels and manifest 100% voxel fractional ventilation. This is the case borne out at the center of the trachea within the voxel fractional ventilation maps of Fig. 1, *b1–b3*, and Fig. 2, *b1–b3*.

Alveolar elements downstream of constricted airways should be deprived of ventilation. If the inhaled gas volume is constant, conservation of mass dictates that alveolar elements distal to non-constricted or less constricted airways should compensate by accommodating larger volumes of gas. Thus the voxel fractional ventilation histogram of a bronchoconstricted lung should indicate an increase in underventilated units as well as the emergence of hyperventilated units. The histograms in Fig. 3 reflect this behavior. We note that Haczku et al. (18) recently used an HP ^{3}He multibreath wash-in approach to quantify ventilation distribution in healthy and allergen-sensitized mice. Their ventilation histograms in the allergen-sensitized mice did show elevations in hypoventilated voxels but not a concurrent increase in more highly ventilated voxels. We are unable to explain this discrepancy.

Heterogeneity quantification. By reporting statistics on the CoV calculated at the level of a small ROI located around each voxel, our intent is to characterize heterogeneity on a local level. The need to apply a local index is illustrated through the first two bar charts in Fig. 7. In each bar chart, the abscissa represents an arbitrary spatial dimension and the ordinate represents an arbitrary signal. In Fig. 7*B*, numbers between 0.7 and 1.0 were randomly generated and then rearranged to form a hill-like distribution in Fig. 7*A*. Despite the fact that Fig. 7*B* is visually heterogeneous while Fig. 7*A* is more homogeneous, these two bar charts would produce the same statistical index if all their elements were included in the computation. Figure 7*C* plots the same information as Fig. 7*B*, except that each bar has 0.6 subtracted from its value in Fig. 7*B*. Figure 7*C* has higher visual heterogeneity than Fig. 7*B* because its signal fluctuation is a higher fraction of the mean signal. This supports our opinion that the CoV is more appropriate for evaluating heterogeneity than standard deviation. The same amount of signal fluctuation in a region of higher signal would correspond to a lower level of heterogeneity compared with the same signal fluctuation in a region of lower signal.

There have been instances when heterogeneity was evaluated by computing CoV on a local scale. In one case, evalu-

Table 2. *Heterogeneity scores at various experiment stages and the corresponding maneuver-induced heterogeneity score changes*

Subject	$\hat{H}_{pre\text{-}MCh}$	$\hat{H}_{post\text{-}MCh}$	$\hat{H}_{post\text{-}DI}$	ΔH_{MCh}	ΔH_{DI}
			Healthy subjects		
HEAL1	0.2760	0.5681	0.4066	0.2921	−0.1615
HEAL2	0.2351	0.3530	0.2813	0.1179	−0.0717
HEAL3	0.2560	0.4164	0.3290	0.1604	−0.0874
HEAL4	0.3144	0.5063	0.3756	0.1919	−0.1307
HEAL5	0.2571	0.4704	0.3509	0.2133	−0.1195
HEAL6	0.2629	0.4871	0.3947	0.2242	−0.0924
			Asthmatics subjects		
RA1	0.4500	0.5564	0.5373	0.1064	−0.0191
RA2	0.3171	0.3652	0.3278	0.0481	−0.0374
RA3	0.3320	0.5488	0.4365	0.2168	−0.1123
RA4	0.2858	0.3971	0.3808	0.1113	−0.0163
RA5	0.3267	0.3685	0.3628	0.0418	−0.0057
RA6	0.2443	0.4403	0.3877	0.1960	−0.0526
RA7	0.2886	0.3803	0.3953	0.0917	0.0150
RA8	0.3297	0.5040	0.5242	0.1743	0.0202
RA9	0.3589	0.5093	0.4052	0.1504	−0.1041
RA10	0.2673	0.5050	0.3914	0.2377	−0.1136

Heterogeneity scores ($\hat{H}$) were determined before (pre-MCh) and after (post-MCh) bronchial challenge with methacholine (MCh) and after a series of deep inspirations (post-DI). The changes in $\hat{H}$ (ΔH) after the MCh challenge and after DIs were computed.

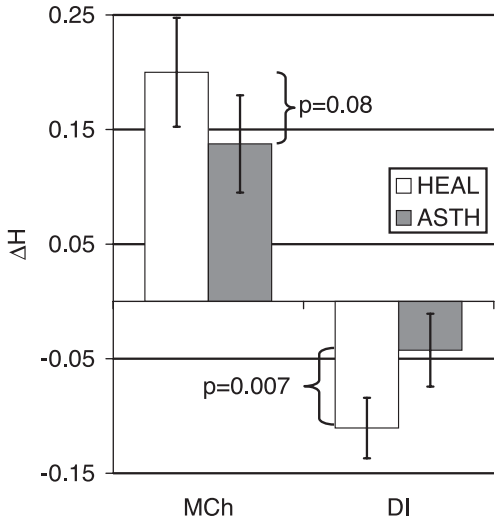

Fig. 5. Changes in heterogeneity scores (ΔH) due to MCh challenge and DIs in asthmatics and nonasthmatics. There is no significant difference in the bronchial challenge-induced ventilation heterogeneity increase between healthy and asthmatic subjects. There is, however, a significant difference in the ventilation heterogeneity reduction brought about by DIs in the 2 subject groups.

ating CoV for adjacent clusters of $3 \times 3 \times 6$ isometric voxels ignored the fact that each voxel contributes to the heterogeneity characteristic of all clusters of which it is a member (47). In another study, insufficient information was provided with regard to the manner in which the clustering was performed (33).

With no precedent for defining a "local" length scale for the lung, we employed a concept widely utilized in fluid mechanics and defined our L as one order of magnitude smaller than the global length scale, or 10% of the lung width. Mapping out the heterogeneity and calculating a heterogeneity index for each slice could be achieved with any other definition of a local length scale. It is conceivable that the selection of a length scale other than that used in this study could lead to heterogeneity changes of different statistical significance. If a local length scale, or a voxel neighborhood over which heterogeneity is evaluated, could be defined with rigorous physiological or anatomical reason, then the resulting heterogeneity map and indexes would have corresponding implications. Thus the behavior of ventilation heterogeneity on different length scales is recommended as a topic for future study and may lead to insight as to the involvement of different sized airways in the bronchoconstriction process.

Edge effects can be seen in the heterogeneity maps. This is best visualized in Fig. 1*c1*. For these coronal slices, despite a visually homogenous voxel fractional ventilation distribution as shown in Fig. 1, *a1* and *b1*, Fig. 1*c1* has a blue-green boundary at the edges of a predominantly dark blue heteroge-

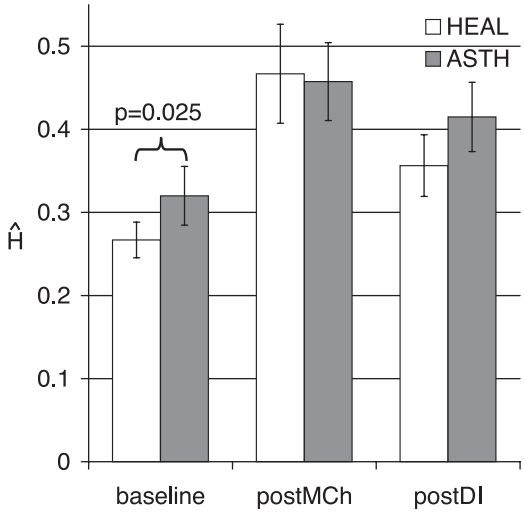

Fig. 4. Heterogeneity scores ($\hat{H}$) at baseline, post-MCh, and post-DI. A statistically significant difference in the baseline heterogeneity score exists between healthy (HEAL) and asthmatic (ASTH) subjects.

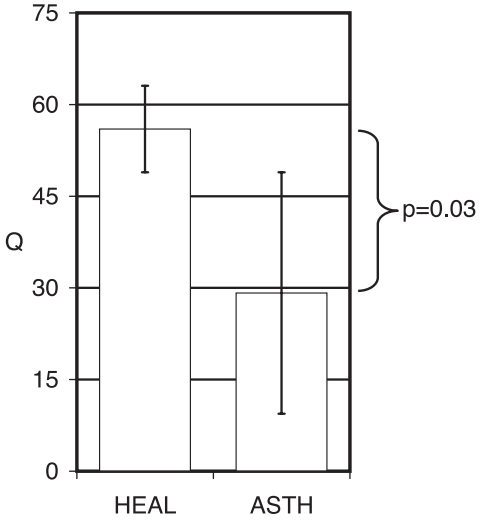

Fig. 6. Statistically significant differences in heterogeneity recovery indexes (Q) also distinguish asthmatics and nonasthmatics.

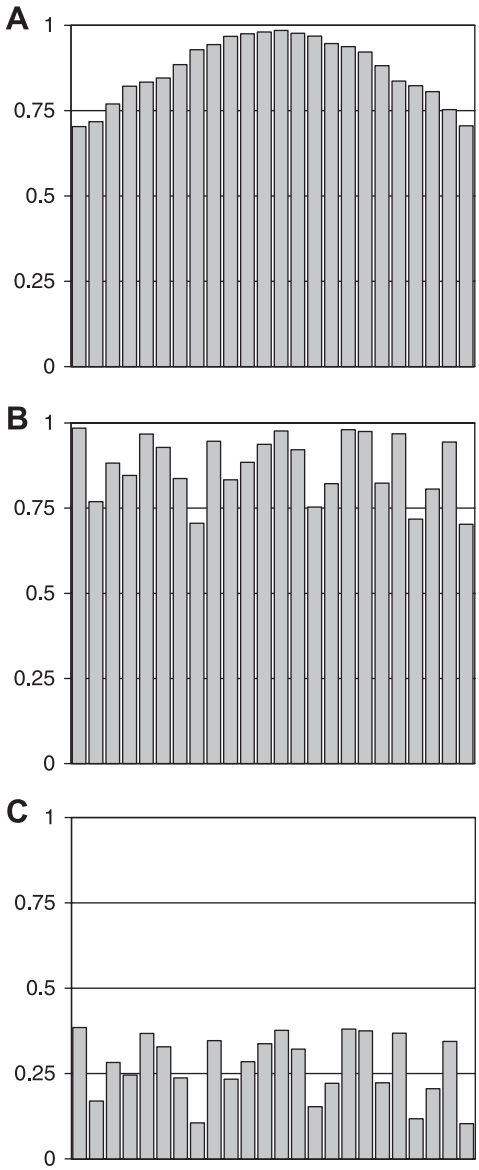

Fig. 7. *A*: randomly generated numbers between 0.7 and 1.0 arranged in a hill-like distribution. *B*: the original randomly generated numbers between 0.7 and 1.0. *C*: randomly generated numbers between 0.7 and 1.0, now with 0.6 uniformly subtracted from each unit. If evaluated on the global level, *A* and *B* would have the same heterogeneity, even though *B* "looks" more heterogeneous. If standard deviations were used to evaluate heterogeneity, *C* and *B* would have the same nonuniformity, even though the signal fluctuation occupies a larger fraction of the signal in *C*.

neity map. This is likely due to the lesser number of pixels in the neighborhood of the pixels of interest toward the rim of the lungs, thereby resulting in higher standard deviations. However, since this phenomenon is present in all three stages of the experiment, its effect should cancel out when images from one stage to another are compared.

Ventilation heterogeneity should not only be a 2-D phenomenon observed in coronal images but a 3-D phenomenon, as well. However, because the anterior-posterior dimension of the voxels was 7.2 times that of the in-plane resolution, this study was limited to evaluating 2-D ventilation heterogeneity. Acquiring 3-D isotropic imaging data would enable the extension of this approach to 3-D. Nonrigid registration algorithms might also improve regional comparison by accounting for lung distortion.

Other issues in image acquisition and processing. To the best of our knowledge, there have been two proactive efforts to address the issue of magnetic susceptibility in HP ^{3}He MRI. One of these two approaches involves the injection of a paramagnetic medium in an attempt to equilibrate the magnetic susceptibility properties of the blood vessels with that of the respiratory system (44). Although successful, this method's invasive nature makes it unlikely to be approved for human experiments. The other approach involves two additional scans with slice refocusing gradients of different lengths, acquiring images that could be used to compensate for the signal lost due to magnetic susceptibility effects (45). For our study, the HP ^{3}He cost and concerns of this approach were similar to those for obtaining P_{O_2} information, and thus the approach was unfeasible.

Although lung tissue/vasculature is not differentiated from poorly ventilated or unventilated regions and in the manual segmentation process, they are not expected to affect the observations in this study. Lung tissue/vasculature exists in all stages of the experiments and thus should lead to a bias error, which cancels out when changes between stages of the experiments are examined. On the other hand, regions deprived of ventilation may experience changes in perfusion. This, in conjunction with magnetic susceptibility effects, may numerically accentuate or depress the computed ventilated heterogeneity. The exact manner and specific quantities by which these effects occur were not investigated.

It is possible that the results of this analysis could become more accurate with the employment of more sophisticated image coregistration approaches that take into account rotation of the lungs as they go from one stage of the experiment to another. Another important factor is the heterogeneous distribution of deflation and hyperinflation throughout the lung, which will require nonrigid coregistration algorithms. However, the absence of visible physical features in the location of ventilation defects will be a great obstacle for such an effort.

Subjectivity of the person processing the images is likely to cause only a small impact. We found a small degree of interuser variability, which mostly could be attributed to the differences between ROIs selected by the various users. Pixel intensities become much lighter toward the borders of the lungs or wherever partial volume effects are expected. Thus the highest uncertainty in the image processing is associated with the judgment of the different operators regarding where the lung boundary is. This was reflected in the voxel fractional ventilation histograms generated by the different image processing software operators, where the most significant differences were for the element corresponding to the lowest intensity pixels. However, despite differences in ROI selection, the approaches in this study still generated voxel fractional ventilation histograms and heterogeneity scores whose behaviors were consistent regardless of the software operator.

Finally, flexible quadrature wrap-around lung coils may not deliver radio frequency (RF) power uniformly to the lungs, and the distribution may differ from subject to subject. The RF field homogeneity has not been quantified. Thus the possible local over- or underestimations of voxel fractional ventilation will not have been corrected for this effect.

Summary. We have developed image processing algorithms to quantify both voxel fractional ventilation distribution and ventilation heterogeneity in healthy and asthmatic subjects using HP ^{3}He MRI. The proposed methodology enables quantification of ventilation in human subjects, given the constraints of subject safety and HP ^{3}He production. Also, we suggest that the signal CoV in the neighborhood of the pixel of interest, which physically represents the signal fluctuation as a fraction of the characteristic signal on a local level, should be the index of ventilation heterogeneity. Our pilot study found that asthmatics start out with a level of ventilation heterogeneity that is higher than that of healthy subjects. When withholding DIs, the healthy subjects had a response to MCh challenge similar to that of asthmatics, corroborating what asthma researchers have determined using nonimaging approaches. We also demonstrated with imaging data that whereas the constricted airways of healthy subjects bronchodilated after DIs, the same effect was greatly limited in asthmatics. These quantitative tools were instrumental in gaining insight into the structure-function relationship of airways and lung periphery in asthmatics and might facilitate further such studies.

REFERENCES

1. **American Thoracic Society.** Guidelines for methacholine and exercise challenge testing—1999. *Am J Respir Crit Care Med* 161: 309–329, 2000.
2. **Altes TA, Powers PL, Knight-Scott J, Rakes G, Platts-Mills TAE, de Lange EE, Alford BA, Mugler JP 3rd, Brookeman JR.** Hyperpolarized ^{3}He MR lung ventilation imaging in asthmatics: preliminary findings. *J Magn Reson Imaging* 13: 378–384, 2001.
3. **Brusasco V, Crimi E, Barisione G, Spanevello A, Rodarte JR, Pellegrino R.** Airway responsiveness to methacholine: effects of deep inhalations and airway inflammation. *J Appl Physiol* 87: 567–573, 1999.
4. **Chen BT, Johnson GA.** Dynamic lung morphology of methacholine-induced heterogeneous bronchoconstriction. *Magn Reson Med* 52: 1080–1086, 2004.
5. **Colebatch HJH, Finugane KE, Smith MM.** Pulmonary conductance and elastic recoil relationships in asthma and emphysema. *J Appl Physiol* 34: 143–153, 1973.
6. **De Lange EE, Altes TA, Patrie JT, Gaare JD, Knake JJ, Mugler JP 3rd, Platts-Mills TAE.** Evaluation of asthma with hyperpolarized helium-3 MRI: correlation with clinical severity and spirometry. *Chest* 130: 1055–1062, 2006.
7. **De Lange EE, Altes TA, Patrie JT, Parmar J, Brookeman JR, Mugler JP 3rd, Platts-Mills TAE.** The variability of regional airflow obstruction within the lungs of patients with asthma: assessment with hyperpolarized helium-3 magnetic resonance imaging. *J Allergy Clin Immunol* 119: 1072–1078, 2007.
8. **De Lange EE, Mugler JP 3rd, Brookeman JR, Knight-Scott J, Truwit JD, Teates CD, Daniel TM, Bogorad PL, Cates GD.** Lung air spaces: MR imaging evaluation with hyperpolarized ^{3}He gas. *Radiology* 220: 851–857, 1999.
9. **Deninger AJ, Eberle B, Ebert M, Grossmann T, Hanisch G, Heil W, Kauczor HU, Markstaller K, Otten E, Schreiber W, Surkau R, Weiler N.** ^{3}He-MRI-based measurements of intrapulmonary pO_2 and its time course during apnea in healthy volunteers: first results, reproducibility, and technical limitations. *NMR Biomed* 13: 194–201, 2000.
10. **Deninger AJ, Mansson S, Petersson JS, Pettersson G, Magnusson P, Svensson J, Fridlund B, Hansson G, Erjefeldt I, Wollmer P, Golman K.** Quantitative measurement of ventilation using ^{3}He MRI. *Magn Reson Med* 48: 223–232, 2002.
11. **Fischer MC, Kadlecek S, Yu J, Ishii M, Emami K, Vahdat V, Lipson DA, Rizi RR.** Measurements of regional alveolar oxygen pressure using hyperpolarized ^{3}He MRI. *Acad Radiol* 12: 1430–1439, 2005.
12. **Fischer MC, Spector ZZ, Ishii M, Yu J, Emami K, Itkin M, Rizi R.** Single-acquisition sequence for the measurement of oxygen partial pressure by hyperpolarized gas MRI. *Magn Reson Med* 52: 766–773, 2004.
13. **Fish JE, Ankin MG, Kelly JF, Peterman VL.** Regulation of bronchomotor tone by lung inflation in asthmatic and non-asthmatic subjects. *J Appl Physiol* 50: 1079–1086, 1981.
14. **Gillis HL, Lutchen KR.** Airway remodeling in asthma amplifies heterogeneities in smooth muscle shortening causing hyperresponsiveness. *J Appl Physiol* 86: 2001–2012, 1999.
15. **Glenny RW, Lamm WJE, Albert RK, Robertson HT.** Gravity is a minor determinant of pulmonary blood flow distribution. *J Appl Physiol* 71: 620–629, 1991.
16. **Gudbjartsson H, Patz S.** The Rician distribution of noisy MRI data. *Magn Reson Med* 34: 910–914, 1995.
17. **Guenther D, Eberle B, Hast J, Lill J, Markstaller K, Puderbach M, Schreiber WG, Hanisch G, Heussel CP, Surkau R, Grossmann T, Weiler N, Thelen M, Kauczor HU.** ^{3}He MRI in healthy volunteers: preliminary correlation with smoking history and lung volumes. *NMR Biomed* 13: 182–189, 2000.
18. **Haczku A, Emami K, Fischer MC, Kadlecek S, Ishii M, Panettieri RA, Rizi RR.** Hyperpolarized ^{3}He MRI in asthma: measurements of regional ventilation following allergic sensitization and challenge in mice. *Acad Radiol* 12: 1362–1370, 2005.
19. **Happer W, Miron E, Schaefer S, Schreiber D, van Wijngaarden WA, Zeng X.** Polarization of the nuclear spins of noble gas atoms by spin exchange with optically pumped alkali metal atoms. *Physiol Rev* 29: 3092–3110, 1984.
20. **Henkelman RM.** Measurement of signal intensities in the presence of noise in MR images. *Med Phys* 12: 232–233, 1985.
21. **Horsfield K, Cumming G.** Morphology of the bronchial tree in man. *J Appl Physiol* 24: 373–383, 1968.
22. **Kauczor HU, Hofmann D, Kreitner KF, Nilgens H, Surkau R, Heil W, Potthast A, Knopp MV, Otten EW, Thelen M.** Normal and abnormal pulmonary ventilation: visualization at hyperpolarized He-3 MR imaging. *Radiology* 201: 564–568, 1996.
23. **Lewis SM, Evans JW, Jalowayski AA.** Continuous distributions of specific ventilation recovered from inert gas washout. *J Appl Physiol* 44: 416–423, 1978.
24. **Lewis SM.** Emptying patterns of the lung studied by multiple-breath N_2 washout. *J Appl Physiol* 44: 424–430, 1978.
25. **Light RW, George RB, Meneely GR, Chouest LJ, Rosekrans RH.** A new method for analyzing multiple-breath nitrogen washout curves. *J Appl Physiol* 48: 265–272, 1980.
26. **Lutchen KR, Yang K, Kaczka DW, Suki B.** Optimal ventilation waveforms for estimating low-frequency respiratory impedance. *J Appl Physiol* 75: 478–488, 1993.
27. **Lutchen KR, Gillis HL.** Relationship between heterogeneous changes in airway morphometry and lung resistance and elastance. *J Appl Physiol* 83: 1192–1201, 1997.
28. **Marcucci C, Nyhan D, Simon BA.** Distribution of pulmonary ventilation using Xe-enhanced computed tomography in prone and supine dogs. *J Appl Physiol* 90: 421–430, 2001.
29. **Melsom MN, Kramer-Johansen J, Flatebo T, Muller C, Nicolaysen G.** Distribution of pulmonary ventilation and perfusion measured simultaneously in awake goats. *Acta Physiol Scand* 159: 199–208, 1997.
30. **Mijailovich SM, Treppo S, Venegas JG.** Effects of lung motion and tracer kinetics corrections on PET imaging of pulmonary function. *J Appl Physiol* 82: 1154–1162, 1997.
31. **Mure M, Domino KB, Lindahl SGE, Hlastala MP, Altemeier WA, Glenny RW.** Regional ventilation-perfusion distribution is more uniform in the prone position. *J Appl Physiol* 88: 1076–1083, 2000.
32. **National Heart, Lung, and Blood Institute.** *Guidelines for the Diagnosis and Management of Asthma* (NIH Publication 97-4051). Bethesda, MD: National Institutes of Health, 1997.
33. **Robertson HT, Altemeier WA, Glenny RW.** Physiological implications of the fractal distribution of ventilation and perfusion in the lung. *Ann Biomed Eng* 28: 1028–1031, 2000.
34. **Robertson HT, Glenny RW, Stanford D, McInnes LM, Luchtel DL, Covert D.** High-resolution maps of regional ventilation utilizing inhaled fluorescent microspheres. *J Appl Physiol* 82: 943–953, 1997.
35. **Robertson HT, Kreck TC, Krueger MA.** The spatial and temporal heterogeneity of regional ventilation: comparison of measurements by two high-resolution methods. *Respir Physiol Neurobiol* 148: 85–95, 2005.
36. **Saam B, Happer W, Middleton H.** Nuclear relaxation of ^{3}He in the presence of O_2. *Physiol Rev* 52: 862–865, 1995.
37. **Salerno M, Altes TA, Brookeman JR, de Lange EE, Mugler JP 3rd.** Dynamic spiral MRI of pulmonary gas flow using hyperpolarized ^{3}He: preliminary studies in healthy and diseased lungs. *Magn Reson Med* 46: 667–677, 2001.

38. **Salerno M, Altes TA, Mugler JP 3rd, Nakatsu M, Hatabu H, de Lange EE.** Hyperpolarized noble gas MR imaging of the lung: potential clinical applications. *Eur J Radiol* 40: 33–44, 2001.
39. **Samee S, Altes T, Powers P, de Lange EE, Knight-Scott J, Rakes G, Mugler JP 3rd, Ciambotti JM, Alford BA, Brookeman JR, Platts-Mills TAE.** Imaging the lungs in asthmatic patients by using hyperpolarized helium-3 magnetic resonance: assessment of response to methacholine and exercise challenge. *J Allergy Clin Immunol* 111: 1205–1211, 2003.
40. **Skloot G, Permutt S, Togias A.** Airway hyperresponsiveness in asthma: a problem of limited smooth muscle relaxation with inspiration. *J Clin Invest* 96: 2393–2403, 1995.
41. **Tsunoda S, Young AC, Martin CJ.** Emptying pattern of lung compartments in normal man. *J Appl Physiol* 32: 644–649, 1972.
42. **Tzeng YS.** *Relating Lung Structure and Function in Asthma Using Hyperpolarized ^{3}He MRI* (PhD thesis). Boston, MA: Boston University, 2007.
43. **Verbanck S, Paiva M.** Model simulations of gas mixing and ventilation distribution in the human lung. *J Appl Physiol* 69: 2269–2279, 1990.
44. **Vignaud A, Maitre X, Guillot G, Durand E, de Rochefort L, Robert P, Vives V, Santus R, Darrasse L.** Magnetic susceptibility matching at the air-tissue interface in rat lung by using a superparamagnetic intravascular contrast agent: influence on transverse relaxation time of hyperpolarized helium-3. *Magn Reson Med* 54: 28–33, 2005.
45. **Wild JM, Fichele S, Woodhouse N, Paley MNJ, Swift A, Kasuboski L, van Beek EJR.** Assessment and compensation of susceptibility artifacts in gradient echo MRI of hyperpolarized 3He gas. *Magn Reson Med* 50: 417–422, 2003.
46. **Wilson TA, Beck KC.** Contributions of ventilation and perfusion inhomogeneities to the VA/Q distribution. *J Appl Physiol* 72: 2298–2304, 1992.
47. **Xu J, Moonen M, Johansson A, Gustafsson A, Bake B.** Quantitative analysis of inhomogeneity in ventilation SPET. *Eur J Nucl Med Mol Imaging* 28: 1795–1800, 2001.
48. **Yamada Y, Burnham C, Hales CA, Venegas JG.** Regional mapping of gas transport during high-frequency and conventional ventilation. *J Appl Physiol* 66: 1209–1218, 1989.